Final Report for Texas AQRP Project 16-031 Condensed Chemical Mechanisms for Ozone and Particulate Matter Incorporating the Latest in Isoprene Chemistry

Submitted to:
Dr. Elena McDonald-Buller, Project Manager Texas Air Quality Research Program The University of Texas at Austin

Submitted by:
University of North Carolina – Chapel Hill
William Vizuete, Jason D. Surratt, Yuzhi Chen, Yue Zhang, Mutian Ma, Zhenfa Zhang
Submitted August 2017

QA Requirements: Audits of Data Quality:
Technical Systems Audits - Not Required for the Project
Audits of Data Quality – 10% Required

Acknowledgement:
The preparation of this report is based on work supported by the State of Texas through the Air Quality Research Program administered by The University of Texas at Austin by means of a Grant from the Texas Commission on Environmental Quality.

Table of Contents

Table of Tables

Table of Figures

Executive Summary

Isoprene is the most abundant non-methane volatile organic compound emitted into the Earth's atmosphere with an annual emission estimated from 500 to 750 Tg [1]. Eastern Texas and northern Louisiana feature some of the largest biogenic emission sources of isoprene in the United States. Recent studies have shown that the atmospheric photo-oxidation of isoprene is a major source of fine particulate matter ($PM_{2.5}$) through the formation of secondary organic aerosol (SOA) particles. In addition, the gas phase oxidation pathways that form SOA precursors can also impact ozone (O_3) production. The goal of the work presented here is an evaluation of the current science on estimation methods for isoprene derived SOA and the gas-phase reactions that produce their precursors. For this evaluation, a modeling system was implemented that incorporated detailed field measurement data and new experimental data was generated aimed at reducing modeling uncertainties. This work directly addresses the stated priority area of improving the understanding of O_3 and $PM_{2.5}$ formation and their interaction with precursors. The goals of the project were achieved through the completion of the following tasks:

- **Task 1:** Updated SAPRC-07 for Isoprene Oxidation Evaluation
- **Task 2:** Laboratory Experiments: The Effects of Particle-Phase Composition, Phase, and Viscosity on IEPOX-Derived SOA Formation
- **Task 3:** Implementation in an Air Quality Model

Task 1 focused on evaluating the state-of-the-science in gas-phase mechanisms in terms of its ability to produce critical SOA precursors and replicate O_3 chemistry. As part of this project the latest version of the SAPRC16 chemical mechanism [2] was evaluated against other mechanisms and with UNC smog chamber data [3, 4]. The chamber data came from 40 experiments (16 characterization runs and 24 isoprene runs) completed at the UNC Dual Smog Chamber Facility (Pittsboro, NC) with isoprene runs that had a range of NO_X (NO_X = NO + NO_2) to isoprene ratios. When compared to the chamber data the SAPRC16 mechanism improves model performance with respect to predictions of peak O_3 and nitric oxide (NO)/nitrogen dioxide (NO_2) crossover times.

The goal of Tasks 2 and 3 were to assess current state of the science models for the prediction of isoprene derived SOA. Specifically, this work focused on the isoprene epoxydiols (IEPOX)- derived SOA formation chemical pathway. In summary, this chemical pathway begins with reactions with the hydroxyl radical (OH) under low NO conditions producing isoprene hydroxyl hydroperoxide (ISOPOOH). ISOPOOH can further react with OH to form IEPOX that then partitions onto pre-existing acidic sulfate aerosol seed forming IEPOX-derived SOA [5-13]. Task 2 produced new data on the impact that organic coatings could have on this uptake process. In current modeling applications the existing sulfate aerosol seed is treated as a homogeneous mixture with reactive parameters derived from empirical data. While in the real atmosphere an aerosol particle can be coated by organic layers formed by gas-phase oxidation of

volatile organic compounds (VOCs) that will change the physical and chemical properties of the seed. Therefore, a more accurate IEPOX-SOA prediction should be achieved by including the effect of coatings on the heterogeneous (multiphase) reactive uptake method.

The critical findings from the experiments in Task 2 included new data showing a strong dependence on aerosol state where the reactive uptake coefficient of IEPOX was reduced by 10 times (compared to pure acidic sulfate aerosol) with only approximately 10 nm of organic coating on existing acidic sulfate aerosol particles. Furthermore, the reduction of the reactive uptake coefficient of IEPOX is non-linear with regards to the SOA coating thickness. Microscopy data was also obtained through existing collaborations that provided evidence for choosing a core-shell morphology resistor coating approach for modeling the acid-catalyzed reactive uptake of IEPOX [14]. These results from task 2 were also used to justify decisions in parameter values for the development of the 0-D model produced in Task 3.

The modeling in Task 3 included the implementation of a heterogeneous reactive uptake coefficient of IEPOX that included the influence of existing organic coatings on IEPOX-SOA formation. All modeling runs relied on field measurements taken during the 2013 Southern Oxidant and Aerosol Study (SOAS) in 2013 at the Look Rock (LRK), Tennessee ground site. For the model it was assumed that the SOA coated acidic sulfate particles has a core-shell morphology and a resistor coating model was adopted [14]. In summary, the model assumes that the formation of IEPOX-derived SOA is predicted as a first order reaction with a heterogeneous reactive uptake that includes several physical and chemical parameters: aerosol acidity, relative humidity (RH), diffusion in particle phase, particle reactivity, the capability that aerosol seeds can absorb mass, and coating effects [15]. The 0-D model was used to predict 2-methyltetrols (tetrols) and organosulfates (IEPOXOS) and found reductions in concentrations when existing coatings were included. Peak tetrol concentrations were reduced by 75% and on average by 30%. IEPOXOS had similar differences with the largest by 62% and on average by 22%. Overall, the modeling showed a 30% reduction in the reactive uptake coefficient of IEPOX across all modeling days.

Key Findings

- Experimental data show measurable reductions in the reactive uptake process of IEPOX to form SOA. The reactive uptake coefficient of IEPOX can be reduced by 10 times with only approximately 10 nm of existing SOA coating.

- The SOA coating thickness and reactive uptake coefficient of IEPOX have a negative correlation relationship. Further, the results show that the reduction of the reactive uptake coefficient is non-linear with regards to SOA coating thickness.

- The level of reduction in the reactive uptake coefficients of IEPOX depends on SOA type. α-Pinene SOA has the smallest reduction while naphthalene SOA has the largest reduction.

- Microscopy data of α-pinene SOA-coated acidic sulfate particles suggests a core-shell morphology.

- A model using a core-shell organic resistor model with consideration of existing SOA coatings improves SOA predictions when compared against field measurements.

- Evaluation of latest SAPRC16 shows improvement when compared with SAPRC-07 in simulating UNC chamber observed peak O_3 and NO/NO_2 crossover times.

Project Deliverables

- Produced modeling system, with integrated experimental data of isoprene photooxidation experiments in the presence of NO_x, for evaluation of the SAPRC16 mechanism.

- Developed and proved a methodology that allows for higher throughput of experiments and effective oxidation of aerosols for systematic understanding of how humidity, chemical composition, and existing SOA coating thickness influence the reactive uptake of gaseous IEPOX into the particle phase to yield new SOA.

- Experimental data on impact on reactive uptake coefficients of IEPOX as a function of three SOA coating types, four SOA coating thicknesses, and three relative humidity levels.

- A 0-D model fully integrated with SOAS field data for predicting heterogeneous IEPOX SOA formation that includes the influence of coatings

Task 1 Updated SAPRC-07 for Isoprene Oxidation Evaluation

Introduction

With previous funding provided by the Air Quality Research Program (AQRP) members of this team evaluated two gas-phase chemical mechanisms: the regulatory version of the condensed SAPRC-07 [16] and an updated version that included isoprene SOA gas-phase precursors for isoprene SOA [17]. The analysis found that the updated SAPRC-07 mechanism produces more O_3 and predicts an earlier NO/NO_2 crossover time than SAPRC-07 for all chamber experiments [18]. Overall, the updated mechanism reacts more VOCs due to a more explicit representation of isoprene oxidation products that increases subsequent OH radical formation[18]. The updated mechanism also increases NO_2 recycling from nitrogen termination species, which accounts for the increase in the afternoon O_3 peak concentrations in the lower-NO_X experiments. This data suggests more work is needed to balance the production of radical and oxidation species to improve O_3 chemistry while maintaining explicit gas-phase precursors for isoprene SOA.

Table 1. Characterization runs with initial concentrations

Date/side	Compound injected	Injection (ppm)	Initial NOx (ppm)	Initial NO (ppm)	Initial NO2 (ppm)
OC0984BLUE	HCHO	0.96	0.5	0.35	0.15
ST3097RED	HCHO	2	0.32	0.27	0.05
ST2396RED	HCHO	0.5	0.33	0.28	0.05
ST2396BLUE	HCHO	1	0.33	0.28	0.05
JL1588RED	HCHO	0.79	0.31	0.22	0.09
JL1588BLUE	HCHO	0.43	0.3	0.21	0.09
AU2497RED	ETHENE	1.92	0.32	0.29	0.03
AU2497BLUE	ETHENE	1.84	0.32	0.29	0.03
AU2393BLUE	ETHENE	0.49	0.33	0.28	0.05
AU1688BLUE	ETHENE	0.97	0.41	0.34	0.07
AU1092RED	METHANE	500	0.35	0.28	0.07
AU1092BLUE	METHANE	250	0.35	0.28	0.07
AU0197RED	METHANE	500	0.35	0.3	0.05
AU0197BLUE	METHANE	250	0.34	0.29	0.05
ST3097BLUE	CO	250	0.33	0.28	0.05
AU3093BLUE	CO	100	0.32	0.28	0.04

Note: Date/side trailing code 'RED' and 'BLUE' denote the side of Dual chamber where the experiment was operated.

Condensed mechanisms, such as the SAPRC-07 [3, 4, 16, 19, 20], are used in regulatory air quality models and have parameters that are highly tuned and any changes may upset the delicate balance of radical and O_3 chemistry. As part of this project data was received from Dr. Carter for the latest version of SAPRC16 chemical mechanism [2]. This yet-to-be released mechanism is the focus of this investigation and its evaluation other mechanisms and the smog chamber data [3, 4]. This evaluation is critical for understanding the performance of this mechanism in relation to its ability to predict critical SOA precursors and ozone.

Methods

Overall, 40 experiments (16 characterization runs and 24 isoprene runs) were conducted in the UNC Dual Smog Chamber Facility (Pittsboro, NC), where the real-time concentration of NOx, VOCs, and O_3 can be measured accurately. Environmental parameters including temperature, relative humidity, and light intensity were also monitored to compute chemical and photochemical reaction rates. Detailed descriptions of the chamber and measurement instruments used can be found elsewhere [21]. Sixteen characterization runs were chosen to evaluate the light model and wall chemistry parameters represented in the auxiliary mechanism. Explanation of the auxiliary mechanism for the UNC smog chamber is available elsewhere [22, 23]. Species in these runs include carbon monoxide (CO), methane (CH_4), ethene (C_2H_4) and formaldehyde (HCHO). These are explicit species in the chemical mechanism whose kinetic information is well constrained. The initial concentrations of these runs are outlined in Table 1.

Table 2 Isoprene runs with initial injected species and concentrations

Date/Side	ISOP/NOx (ppm/ppm)	Initial ISOP (ppm)	Initial NOx (ppm)	Initial NO (ppm)	Initial NO2 (ppm)
JN1793BLUE	0.18	0.1	0.54	0.47	0.07
JN1793RED	0.35	0.19	0.54	0.47	0.07
JL1780RED	0.44	0.2	0.46	0.36	0.1
JN2381BLUE	0.58	0.26	0.45	0.32	0.13
JL2381RED	0.65	0.28	0.43	0.35	0.08
JN2381RED	1.04	0.46	0.44	0.31	0.13
JL1780BLUE	1.11	0.52	0.47	0.36	0.11
JN2697BLUE	1.13	0.38	0.34	0.27	0.07
JN2592RED	1.61	0.58	0.36	0.31	0.05
OC1596BLUE	1.78	0.58	0.33	0.29	0.04
OC1596RED[a]	1.84	0.6	0.33	0.28	0.04
AU0897RED	1.89	1.28	0.68	0.59	0.09
AU1597BLUE	1.9	1.58	0.83	0.78	0.06
JN0298BLUE	2.13	1.5	0.7	0.58	0.12
ST0799BLUE	2.31	1.62	0.7	0.69	0.01
ST1199BLUE	2.47	1.5	0.61	0.6	0.01
JN2996RED	2.53	1.02	0.4	0.33	0.07
AU1196BLUE	2.91	0.98	0.34	0.29	0.04
JN2996BLUE	3.12	1.26	0.4	0.34	0.07
ST2496RED	3.2	2.06	0.64	0.57	0.07
JN2592BLUE	3.33	1.2	0.36	0.32	0.04
JN2697RED	3.73	1.29	0.35	0.28	0.07
OC0697RED	4.85	3.12	0.64	0.56	0.08
ST1199RED	9.29	1.56	0.17	0.16	0.01

[a] 200 ppm CO also injected in this experiment.

Twenty-four isoprene photooxidation experiments were selected and shown in Table 2. In this study, runs in which the isoprene:NOx concentrations have a ratio less than 1.25 (ppm/ppm) were arbitrarily classified as having a low VOC:NOx ratio or a high- NOx experiment, while those over 1.25 were considered to have a high VOC:NOx ratio or a lower-NOx experiment. Note that the term high- or low-NO_x is used in this report as an indication of the relative initial NO_x-to-isoprene ratio of an experiment. The absolute amounts of NOx injections are larger than ambient level.

Three mechanisms were compared in this study: SAPRC-07 [20], the Xie mechanism [17], and SAPRC16 [2]. All three mechanisms were implemented in the UNC Morpho Photochemical Reaction Simulation System [24]. SAPRC-07 source code was created based on Dr. Carter's report [20] and SAPRC16 was provided by via direct communications with Dr. Carter. The Xie mechanism was contained in the CMAQ files provided by Dr. Ying Xie, and converted to the Morpho format [22].

The UNC Auxiliary Mechanism (version-aadg) was used to account for chamber-dependent wall mediated effects [18]. Simulation results of 16 characterization runs used in this study also have satisfactory modeling performance. Based on this evidence it was determined that the representation of the auxiliary mechanism was suitable for this investigation. In addition to the auxiliary mechanism, however, each experiment has

unique injection values of initial loadings of wall water, HONO and wall HNO_3. These are dependent on the amount of time the chamber has been vented with dry air before the experiment and recent history of experiments conducted in the chamber before that experiment.

Results

Simulations with SAPRC-07, the Xie mechanism, and SAPRC16 were statistically compared with observational data in terms of peak O_3 concentration and NO/NO_2 crossover time derived from temporal concentration profiles of NO, NO_2, and O_3. The NO/NO_2 crossover time is the length of time it takes for NO and NO_2 concentrations to converge since sunrise. It implies how fast a mechanism is converting NO to NO_2 and propagating the autocatalytic process of O_3 production. Ozone peak/maximum value is a direct indicator of regulatory interest as reflected by 8-h O_3 standard in NAAQS. Both NO/NO_2 crossover time and O_3 peak/maximum are reported in the form of normalized mean bias (NMB).

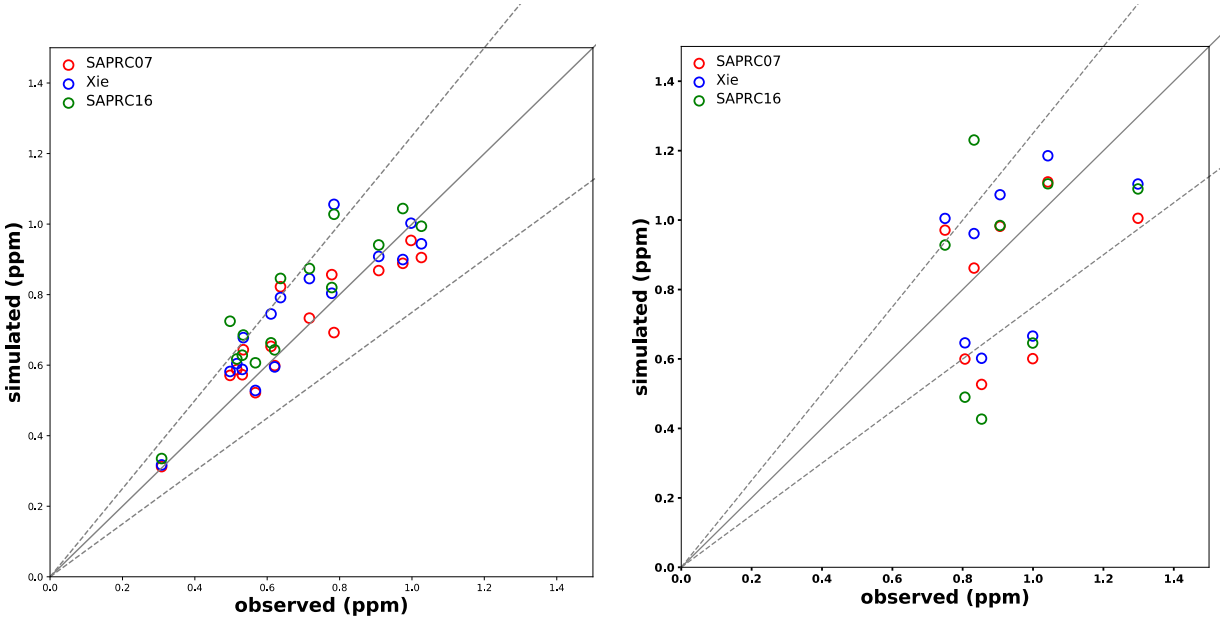

Figure 1 Ozone peak (left) under low isoprene:NOx ratio and (right) under high isoprene:NOx ratio. Each circle represents the peak ozone for each experiment, with the predicted value on the y axis and measured value on the x axis. The diagonal line suggests perfect model agreement with the observation. Red Circle stands for ozone concentration simulated by SAPRC07, blue circle stands for predictions by the Xie mechanism, and green circle stands for predictions by SAPRC16 mechanism. The area enclosed by two dashed lines at ±25% range of bias.

Figure 1 shows the simulated O_3 peak concentration values plotted against observational values. For chamber VOC(s)+NOx daytime experiments, the observed pattern of O_3 temporal profile changes with relative NOx abundance. A lower-NOx

experiment is often characteristic of two O_3 peaks, of which the second peak is due to photolysis of NO_2 recycled back from reservoir species like peroxy acyl nitrates (PAN). Reported here are only the graphical results of the first/morning O_3 peak due to direct O_3 photochemistry.

Under both high- and low-NOx conditions, the Xie O_3 peak was consistently higher than the peak predicted with SAPRC-07 by as much as 20%. The difference was most pronounced under high-NOx conditions. Likewise, the SAPRC16 predictions were also consistently higher in the lower NOx experiments relative to SAPRC-07. In many of the experiments SAPRC16 made more O_3 than the Xie mechanism. As shown in Table 3 this resulted in a 13% increase in NMB to 18.2% compared to SAPRC-07. The SARPC16 mechanism evaluated against the high-NOx experiments were mixed relative to SAPRC-07, but did improve NMB as shown in Table 3 by 3%. It is important to note that, under lower-NOx conditions, both mechanisms were pushing model performance in the wrong direction, increasing bias of first O_3 peak. Although there are insufficient number of runs in the high-NOx experiments to conclude a statistically significant difference in the two mechanisms.

Table 3 Summary of ozone peak model performance statistics

Experiment	Condition	Mechanism	NMB (%)	R^2	P value
N=8	High NOx	SAPRC-07	-9.80	0.13	0.38
		Xie	-1.99	0.16	0.41
		SAPRC16	-6.79	0.11	0.33
N=16	Lower NOx	SAPRC-07	4.92	0.85	3.96E-07
		Xie	9.44	0.79	4.00E-06
		SAPRC16	18.23	0.76	1.14E-05

Figure 2 shows the observed NO/NO_2 crossover time versus simulated results across 8 high-NOx experiments and 16 lower-NOx experiments. All three mechanisms under-predict NO/NO_2 crossover time relative to measurements from the lower-NOx experiments. The Xie mechanism always had an earlier crossover time than SAPRC-07 and was even earlier for lower-NOx experiments. The SAPRC16 mechanism, as shown in Table 4, predicts a 2% improvement in NMB and overall is the best performing mechanism. The NMB for the SAPRC16 is only -2% versus the high NOx measurements. Detailed statistical results for all three mechanisms are summarized in Table 4.

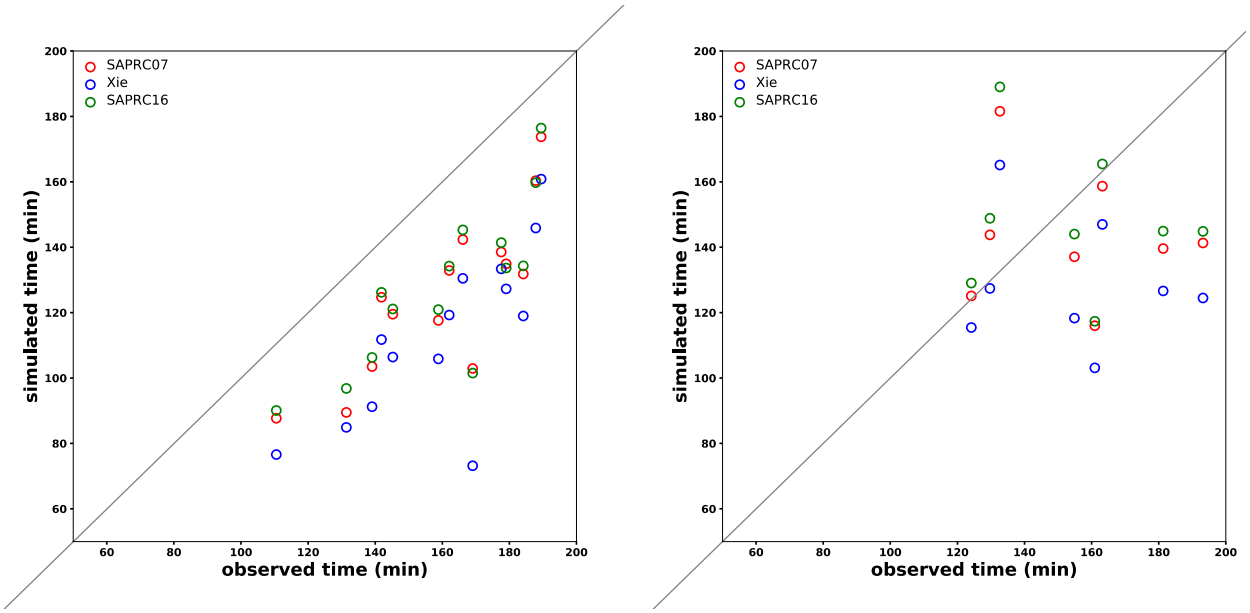

Figure 2 NO to NO_2 cross over times (left) under low isoprene:NOx ratio and (right) under high isoprene:NOx ratio. Each circle represents the peak ozone for each experiment, with the predicted value on the y axis and measured value on the x axis. The diagonal line suggests perfect model agreement with the observation. Red Circle stands for SAPRC07, blue circle stands for the Xie mechanism, and the green circle stands for predictions by SAPRC16 mechanism.

Table 4 Summary of crossover statistics

Experiment	Condition	Mechanism	NMB (%)	R^2	P value
N=8	High NOx	SAPRC-07	-5.45	0.02	7.29E-01
		Xie	-14.94	0.03	6.79E-01
		SAPRC16	-2.08	0.02	7.12E-01
N=16	Lower NOx	SAPRC-07	-22.12	0.76	1.06E-05
		Xie	-29.73	0.67	9.62E-05
		SAPRC16	-20.77	0.75	1.46E-05

Case Study

To demonstrate the model performance statistical features for the three mechanisms two representative experiments were chosen – one high-NOx experiment and one lower-NO_X experiment (Table 5). The OC1596RED is a lower NOx experiment where SAPRC16 over predicts peak O_3 even more than the other two mechanisms. The JN2697BLUE is a high-NOx experiment where the SAPRC16 mechanism improves both NO/NO_2 crossover time and peak O_3. The simulated and observed concentrations time profiles are plotted for isoprene, NOx, and O_3 (Figure 3 and Figure 4). Figure 3 shows the isoprene decay for the two experiments with the Xie mechanism oxidizing the most isoprene compared to the other two mechanisms. SAPRC07 and SAPRC16 consumes isoprene closer toward what was observed and the latter performing better in NO/NO_2 crossover time. As for O_3 peak model performance in both cases, the three mechanisms agree with the bulk pattern reflected by the statistical analysis (Table 3).

Table 5 Selected case studies with initial conditions and peak ozone concentrations

Experiment	Initial isoprene:NO_X (ppm/ppm)	Initial isoprene (ppm)	Initial NO_X (ppm)	O_3 peak (ppm)	O_3 max (ppm)
JN2697BLUE	1.13	0.38	0.34	0.91	0.91
OC1596RED	1.84	0.6	0.33	0.72	0.72

Note: Here only the measured values of the first ozone peak are shown.

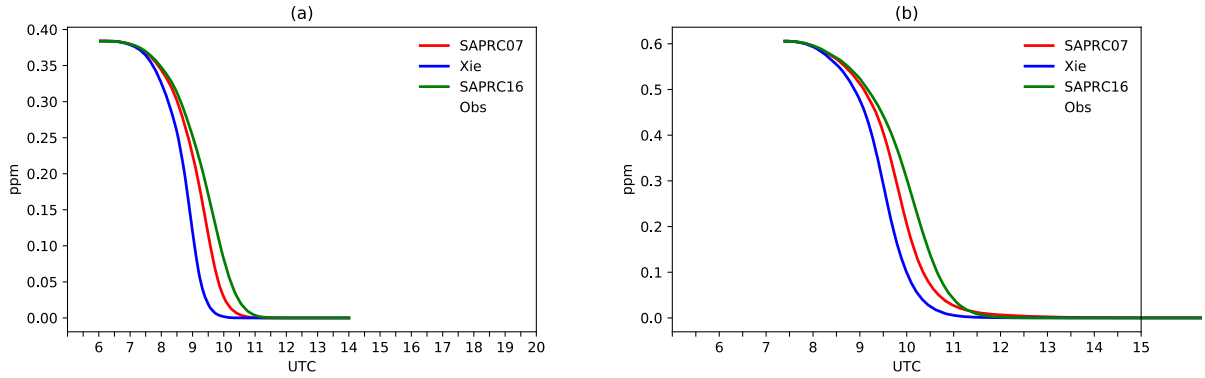

Figure 3 Isoprene concentration time profile for: (a) JN2697BLUE (High NO_X) and (b) OC1596RED (Lower NO_X)

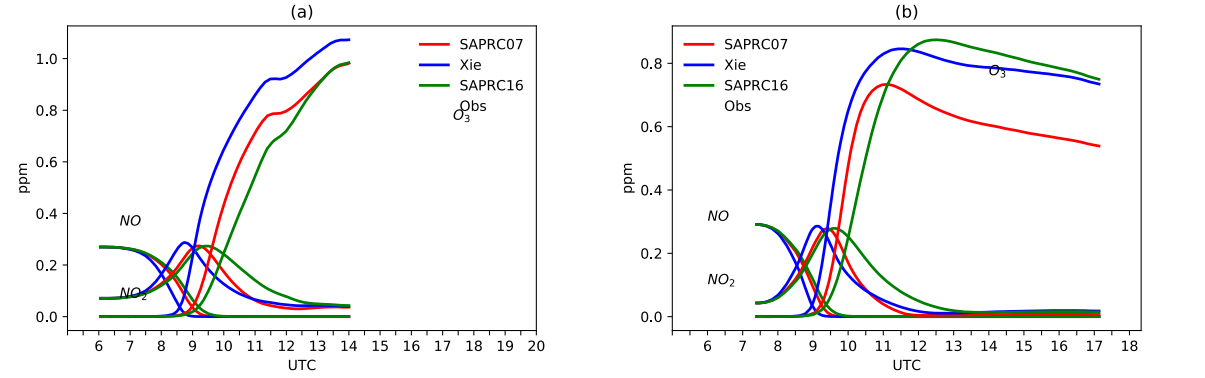

Figure 4 Ozone and NOX concentration time profile for: (a) JN2697BLUE (High NOX) and (b) OC1596RED (Lower NOX)

Discussion

This report used outdoor chamber experiments to evaluate SAPRC07, SAPRC16, and the Xie mechanisms. The model performance results suggest that the Xie mechanism produces more O_3 and predicts an earlier NO/NO2 crossover time than SAPRC-07 for all experiments. Under lower-NOx conditions, both mechanisms over-predict O_3 observations; the Xie mechanism worsens performance and increases the bias of O_3 from 4.92% to 9.44%. Overall, the Xie mechanism reacts more VOCs due to a more explicit representation of isoprene oxidation products and therefore increases subsequent OH formation. The latest chemical mechanism, as represented by SAPRC16, improves model performance relative to the SAPRC-07 mechanism in terms of replicating O_3 and maintaining critical precursors needed for isoprene-derived SOA.

Task 2 Laboratory Experiments: Particle-Phase Composition, Phase, and Viscosity on IEPOX Multiphase Chemistry

Introduction

Oxidized organic species comprise a large fraction (20-80%) of submicron atmospheric aerosol particulate matter (PM), especially outside of heavily populated urban areas and intensive industrial regions [25]. Secondary organic aerosol (SOA) consists of a large mass fraction of the organic PM, formed by the oxidation of volatile and semivolatile organic gaseous species. These secondary oxidation products condense on pre-existing aerosol particles or nucleate with other pollutants like sulfuric acid to form new particles [26]. SOA is expected to contain thousands of distinct partially oxidized organic compounds that evolve to higher oxidation states as the SOA chemically ages. The aging process includes a combination of (1) heterogeneous oxidation by gaseous photochemical oxidants and (2) more volatile component evaporation followed by further gas-phase oxidation and re-condensation of secondary products [27].

Isoprene is the most abundant non-methane VOC emitted into the Earth's atmosphere with an annual emission estimated from 500 to 750 Tg [1]. Recent studies have shown that the photo-oxidation of isoprene is a major source of SOA in the atmosphere. Laboratory studies have demonstrated that the major pathway involving the formation of isoprene SOA is the reactive uptake of isoprene epoxydiols (IEPOX) onto acidic sulfate particles. This pathway accounts for more than 40% of the total organic aerosols (OA) mass during summer in the southeastern US [15]. Moreover, these acidic sulfate particles are more likely to be coated with existing SOA, which could impact the reactive uptake process of IEPOX into the acidic sulfate particles, depending on the phase state of the organic coating [28, 29].

It was initially assumed that the oxidized organic fraction would be liquid, particularly at high relative humidity where organic and inorganic water-soluble PM components would deliquesce. However, recent evidence has shown that both laboratory-generated and atmospheric SOA particles can be semi-solid or solid. For example, inertial impaction studies have shown that SOA particles formed from biogenic organic precursors produced in the Hyytiälä forest, Finland, bounce upon impact with a solid surface, indicating that these particles are in a solid state, because otherwise liquid organic particles would splatter [30, 31]. It is clear that these solid or semi-solid particles are not organic crystals, because they are created by photochemical processes known to produce a large number of distinct semi-volatile products that co-condense, thereby inhibiting crystallization.

The physical state of the aerosol has a range of atmospherically important effects. Recent studies have confirmed that glassy SOA does have much lower vaporization rates than previously assumed [32, 33] and that this type of SOA strongly influences air quality and climate change issues. There is also convincing evidence that that such glassy SOA are effective ice nucleation agents [30, 34-37]. There have been modeling

results simulating how particle state would limit multiphase chemistry, and how that would subsequently affect the growth and evolution of SOA. Nevertheless, there has been little experimental evidence to support these modeling results. In this study, a state-of-the-art technique and analytical instrumentation at UNC was used to provide experimental data on how SOA coating alters the reactive uptake of IEPOX onto acidic sulfate particles, and the importance of such a process in aerosol formation. Moreover, the team at UNC has sought further collaboration with Aerodyne Research and utilized Aerodyne's potential aerosol mass (PAM) reactor, in order to solve the issue of coating acidic seed particles with different coating thicknesses. The PAM reactor was used instead of a smog chamber to coat acidic sulfate aerosol since it allows for higher throughput of experiments and oxidizes the aerosol more effectively, leading to OA with atomic oxygen-to-carbon (O:C) ratios similar to atmospheric PM [38]. As shown in this report, there has been significant progress in measuring and understanding how humidity, chemical composition, and coating thickness influence the reactive uptake of IEPOX into the particle phase.

Methods

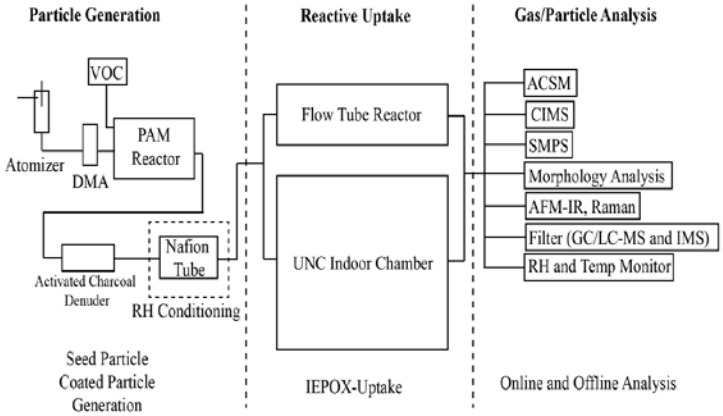

Figure 5 Schematic flow diagram of the reaction setup. The particle generation section uses atomizer and PAM to generate SOA coated acidified ammonium sulfate particles for reactive uptake. A flow tube reactor and environmental chamber are used for the reactive uptake process.

The reactive uptake of IEPOX onto coated acidic seed particles is measured by using a movable injector flow tube setup. The overall setup is shown in Figure 5. Atomized acidic sulfate particles are injected into the PAM. A syringe pump is used to introduce vaporized VOCs into the PAM at a tunable rate. Depending on the reaction, ozonolysis and/or photo-oxidation of the VOCs takes place in the PAM to form organic materials coated onto the existing acidic sulfate particles. The particles are introduced through a charcoal denuder to remove excess gas-phase species in order to prevent secondary reactions inside the flow tube. At the outlet of the flow tube, the remaining unreacted IEPOX is measured by a Time-of-Flight Chemical Ionization Mass Spectrometer (ToF-CIMS). The particles exiting the flow tube are analyzed by scanning mobility particle sizer (SMPS), aerosol chemical speciation monitor (ACSM), filter analysis, scanning electron microscope (SEM) morphology analysis, and chemical property analysis, including electron-diffraction x-ray spectroscopy (EDX) and Raman spectroscopy.

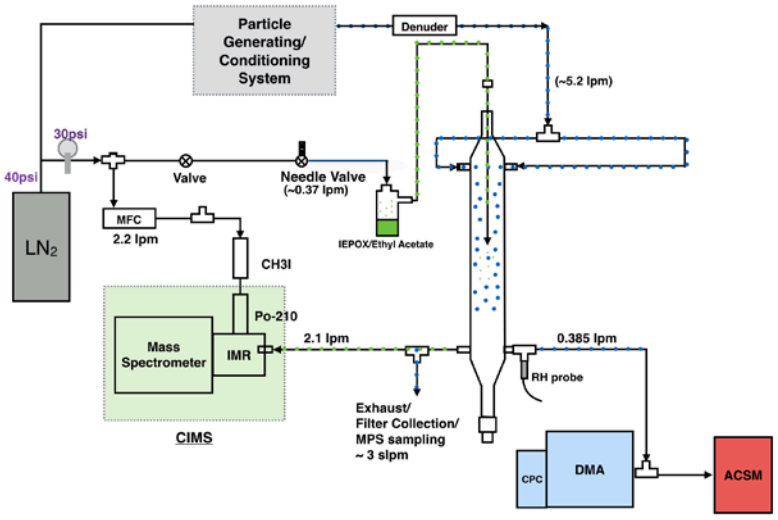

Figure 6 Detailed flow chart when performing the reactive uptake of IEPOX on SOA coated acidified ammonium sulfate particles.

The detailed setup of the movable injector flow tube is described in Figure 6. Various aspects of the flow setup have been modified and improved to better fit the experimental purpose and reduce uncertainties in measurement. As shown in Figure 5, IEPOX is injected into the flow tube through the center injector. Organic-coated acidic sulfate particle flow is split into two streams and is injected from the two sides of the flow tube reactor. By varying the length of the injector inside the flow tube reactor, IEPOX has different reaction times with the aerosol particles, and hence the heterogeneous loss rate coefficient could be calculated by subtracting the wall loss coefficient, k_{wall}, from the total loss rate coefficient, k_{total}, i.e.,

$$k_{het} = k_{total} - k_{wall} \quad (1)$$

After correcting the k_{het} with the non-plug flow condition, the uptake coefficient, γ, could be calculated as

$$\gamma = \frac{4k_{het}}{S_a \omega} \quad (2)$$

where S_a is the total surface area of the aerosol particles and ω is the mean molecular speed of IEPOX molecule in the air [14].

Results

One example of the current results is shown in Figure 7 (the blue line), which demonstrates ToF-CIMS data of IEPOX ion count injector positions at different regions of the flow tube. The figure shows distinctive numbers of ion counts as the injector moves, which is a confirmation of the expected behavior. The IEPOX ion count is divided by the iodide ion (I^-) signal and then averaged over the period of time when the

injector is held stable at each position. The logarithm of normalized IEPOX ion counts are then plotted against the corresponding reaction times of the IEPOX resident in the flow tube, as shown in Figure 4. Based on the pseudo-first order reaction theory, a linear regression is used to fit the data points of each condition, and the slope indicates the uncorrected loss rate coefficient. Figure 8 shows that the uncorrected loss rate coefficients decrease as the SOA coatings increase. By applying equations (1) and (2) together, the uptake coefficient of that specific condition could be calculated.

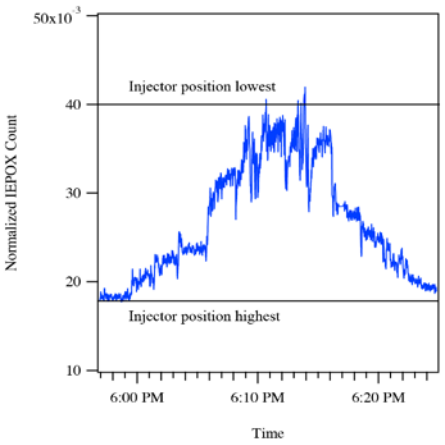

Figure 7 Sample CIMS data of IEPOX+I^- ion when operating the IEPOX uptake inside the flow tube reactor. The position of the injector is shown in the plot.

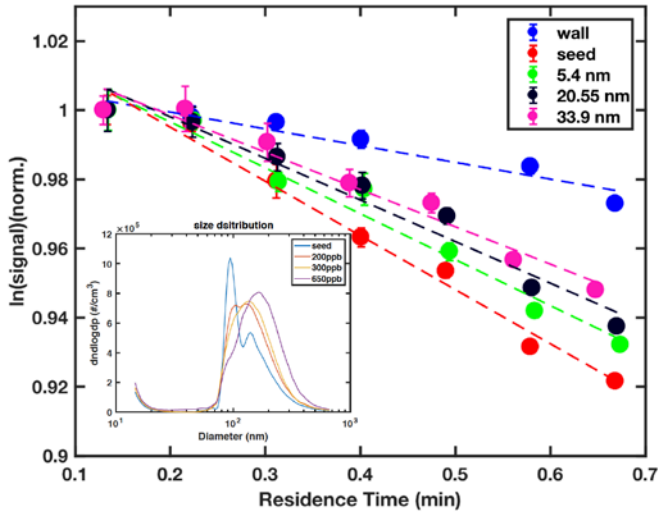

Figure 8 Normalized logarithm of the IEPOX signal versus residence time of the IEPOX inside the flow tube reactor when reacting with α-pinene SOA-coated acidified ammonium sulfate particles. Different colors represent wall uptake and different SOA coating thickness results. The inset plot shows how the number-diameter aerosol distributions of the particles change as the coating thickness increases.

A summary of the experimental conditions used in this study are listed in Table 6. In addition to the pure acidic sulfate seed particles, three other types of SOA are generated to coat the existing acidic sulfate seed particles. The SOA coating thickness

is systematically varied from zero to 20 nm by controlling the precursor concentration, which is controlled by the syringe injector. The humidity level changes from 10% to 50% for each type of SOA by using the dual Nafion tubes.

These three precursors are strong representations of the SOA formed in the ambient environment. α-Pinene ozonolysis SOA is one of the major biogenic SOA [39], while toluene and naphthalene SOA produced from photochemical oxidation are important markers for anthropogenic SOA [39]. Figure 9 shows the reactive uptake coefficient of IEPOX on α-pinene SOA-coated acidic seed particles. It shows that at 15% relative humidity (RH), there is a trend that the IEPOX uptake coefficient decreases with increasing SOA coating thickness. At 30% and 50% RH, the uptake coefficients drop by a factor of 3 and 2, respectively, but remain the same at higher coating thicknesses within the error bar. The results suggest that α-pinene SOA at lower RH does hinder the reactive uptake of IEPOX as coating thickness increases. However, factors of 2-3 reduction are sufficient enough to reduce IEPOX-derived SOA formation (as further discussed below in subsequent sections of this report).

Table 6 Experimental Conditions Used for This Study

Coating SOA Precursor	Concentration (ppb)	Reaction Condition	Coating Thickness (nm)	Relative Humidity (%)
α-pinene	200-650	Ozonolysis		
Toluene	420-1200	Photo-oxidation	0/5/10/15-35	15/30/50
Naphthalene	100-500	Photo-oxidation		

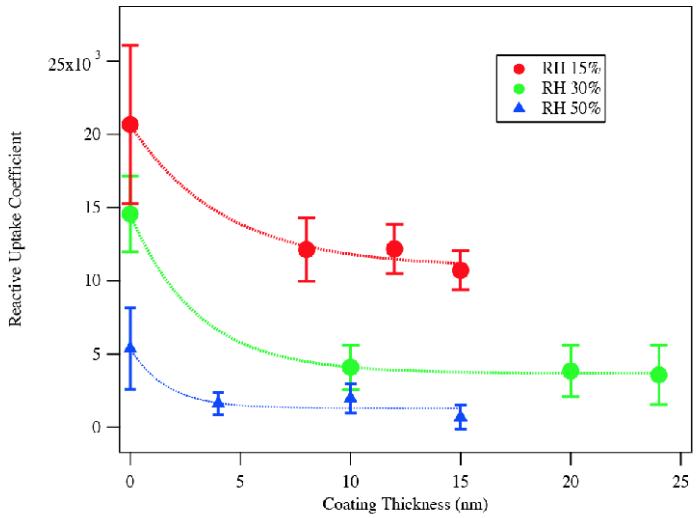

Figure 9 The calculated uptake coefficient as a function of coating thickness for α-pinene ozonolysis coated SOA particles. Different color points represent different humidity levels inside the flow tube reactor when the uptake happened. The shaded area is the fitted trend line.

The reduction is likely caused by reducing the diffusion coefficient of the gas-phase IEPOX into the particle phase. At higher 30 and 50 % RH conditions, the reduction of diffusion coefficient at the coating thickness shown here may not be significant. A thicker coating may have an obvious reduction of IEPOX uptake coefficient at these higher RHs.

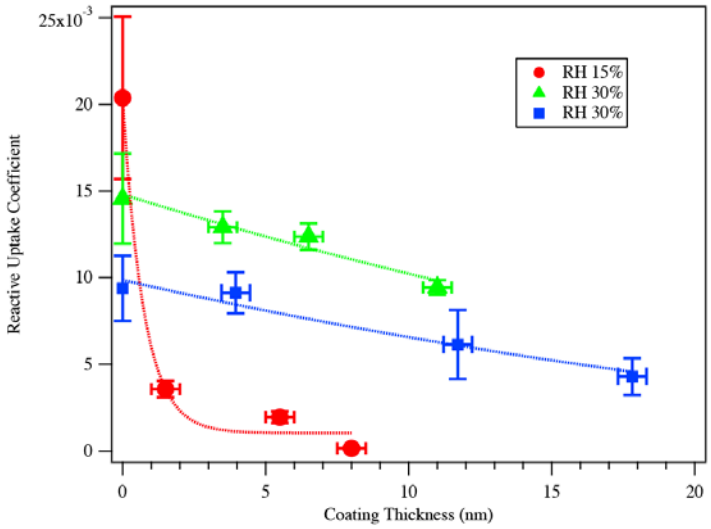

Figure 10 The calculated uptake coefficient as a function of coating thickness for toluene photo-oxidation coated SOA particles. Different color points represent different humidity levels when the uptake happened inside the flow tube reactor. The shaded area is the fitted trend line.

Figure 10 shows how the reactive uptake coefficients of IEPOX change with different coating thickness of toluene SOA onto the acidic seed particles at various RHs. Similar to α-pinene coated SOA results, it also shows that at lower RH, the reactive uptake coefficient decreases with increasing SOA coating, but the reduction effect is much stronger and at only 8 nm coating, the uptake coefficient is almost zero. But different than α-pinene-coated SOA, as the RH becomes higher, the reduction of uptake coefficient still decreases with coating thickness. The trend indicates that the toluene SOA potentially has an even higher viscosity than α-pinene SOA generated from the experiment.

The reactive uptake of IEPOX into naphthalene SOA-coated acidic seed particles are also examined as well and shown in Figure 11. Naphthalene is used here to mimic the SOA produced from polycyclic aromatic hydrocarbons (PAHs). At 15% RH, the reduction of reactive uptake is even lower than that of the toluene SOA coating produced under photooxidation conditions. At 50% RH, naphthalene SOA still shows a strong reduction in the reactive uptake coefficient. These results indicate that naphthalene SOA has an even stronger reduction effect compared with the other two SOA precursors.

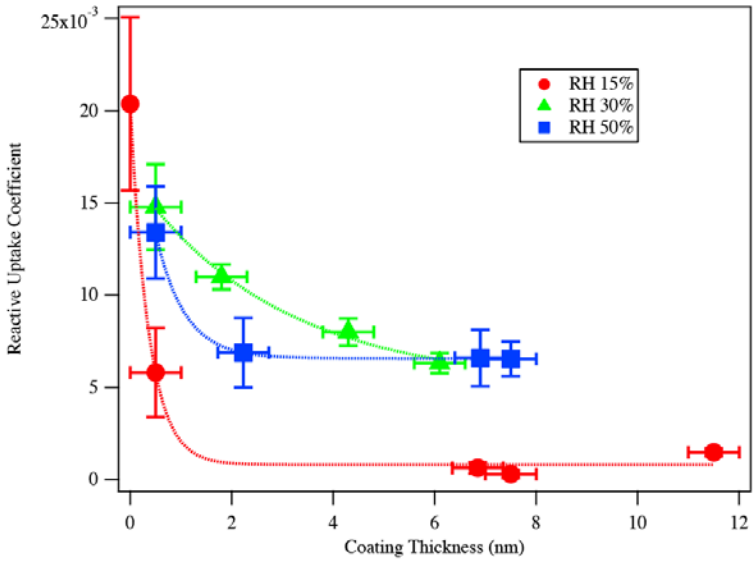

Figure 11 The calculated uptake coefficient as a function of coating thickness for naphthalene photo-oxidation coated SOA particles. Different color points represent different humidity levels when the uptake happened inside the flow tube reactor. The shaded area is the fitted trend line.

Discussion

The reactive uptake of IEPOX on three different SOA precursors were examined in this study. This uptake coefficient is measured as a function of coating thickness and RH, and the results provide valuable information on how SOA type and RH affect the multiphase chemistry of IEPOX leading to isoprene SOA. Key findings from this work include:

1. All types of coatings show measurable reductions in the reactive uptake process of IEPOX. The reactive uptake coefficient can be reduced by 10 times with only approximately 10 nm of coating. The result suggests that multiphase chemistry is strongly dependent on aerosol phase state and needs to be considered in air quality models.

2. The SOA coating thickness and reactive uptake coefficient have a negative correlation relationship. This phenomenon agrees with the hypothesis on how viscosity affects the reactive uptake process: as coating thickness increases, it takes longer for gas molecules (i.e., IEPOX) to travel through the SOA coating to reach the acidic core, thereby reducing the reactive uptake coefficient. However, the results show that the reduction of the reactive coefficient is non-linear with regards to SOA coating thickness. The non-linearity is plausibly caused by coagulation between particles, causing the particles to be non-spherical and deviate from the core-shell structure that is assumed in the calculations used in this work.

3. The level of reduction in the reactive uptake coefficients of IEPOX depends on SOA coating type. The α-pinene SOA has the smallest reduction while naphthalene SOA has the largest reduction when other environmental parameters are the same. The difference in reactive uptake coefficients are most likely to be caused by different SOA viscosities.

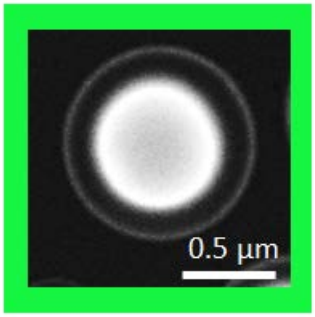

Figure 12 SEM-EDX image of an α-pinene SOA-coated acidic sulfate particle. The brighter color indicates the sulfate and the lighter region around the center is the carbon. This image confirms core-shell morphology.

Besides working the reactive uptake experiments and taking advantage of the research instruments at Aerodyne, the UNC team also extended the scope of this work by collaborating with multiple research groups. The UNC has collaborated with Andrew Ault's group at University of Michigan to study the morphology of the aerosol samples generated from the PAM. The team also works with Aerodyne Research by using ion mobility spectroscopy to study the chemical composition of the SOA and will cross compare the data with the results from electrospray ionization mass spectroscopy at UNC. Importantly, this collaborative work with Professor Andrew Ault's group has revealed through microscopy that α-pinene SOA coated acidic sulfate particles have a core-shell morphology. As shown in Figure 12, SEM-EDX images confirm core-shell morphology of the α-pinene SOA coated acidic sulfate particles. As a result, this informed the use in Task 3 of the core-shell morphology resistor coating model from Gaston et al. [2014]. It was also used to determine the diffusion coefficient of IEPOX in these different SOA coated sulfate particles.

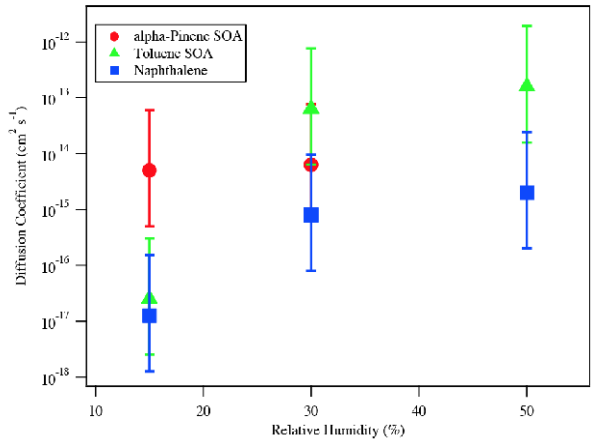

Figure 13 Deduced diffusion coefficients of IEPOX in the different SOA-coated sulfate particles under varying RH conditions. This was derived by assuming the core-shell morphology resistor coating model applied by Gaston et al. [2014].

As shown in Figure 13, the estimated diffusion coefficients of IEPOX into these different SOA coated particles ranges from 10^{-12} to 10^{-18} cm^2 s^{-1}. As a result of these values, the SOA generated under these RH conditions are likely to be semi-solid to solid phase state [40]. For this work a total particle surface area of 10 μm^2 cm^{-3} and the pH of the particles are 1 were assumed. This was based on characteristics of aerosol particles in the southeastern U.S. [41]. The next step was to calculate how much IEPOX-derived SOA would be reduced if the IEPOX uptake coefficient is reduced by half due to an existing SOA coating. As demonstrated in this study, most of the SOA reduced the uptake coefficient of IEPOX by at least a factor of 2. Thus, this is likely a reasonable set of assumptions to conduct a back-of-the-envelope calculation. As a result of these assumptions the IEPOX-derived SOA would decrease by 30%, indicating that SOA coatings likely need to be considered in modeling IEPOX-derived SOA in the atmosphere, especially since most of the experimental data show that the uptake coefficient of IEPOX is reduced by 4-5 times.

Looking towards future experiments and further interpretation of the dependence of SOA type and RH levels on the reactive uptake of IEPOX (Figure 14), efforts have also been focused on combining experimental results and modeling results to generalize the data for broader impacts. For the experimental part, current work focusing on chemical characterization of the organic aerosols in order to link their chemical composition to their phase state. An Aerosol Chemical Speciation Monitor (ACSM) has been used in conjunction with SMPS throughout the experiment. The data from ACSM are currently being analyzed in order to determine the O:C and H:C ratio of the SOA. Filter samples of all the SOA conditions have been collected throughout the experiment as well. The approach is to utilize liquid-phase chromatography/electrospray ionization-high-resolution quadrupole time-of-flight mass spectrometry (LC/ESI-HR-QTOFMS), and gas-phase chromatography/electron ionization-quadruopole mass spectrometry (GC/EI-

MS) to study the chemical composition of the SOA components and identify key species that can influence the phase state of the organic aerosol.

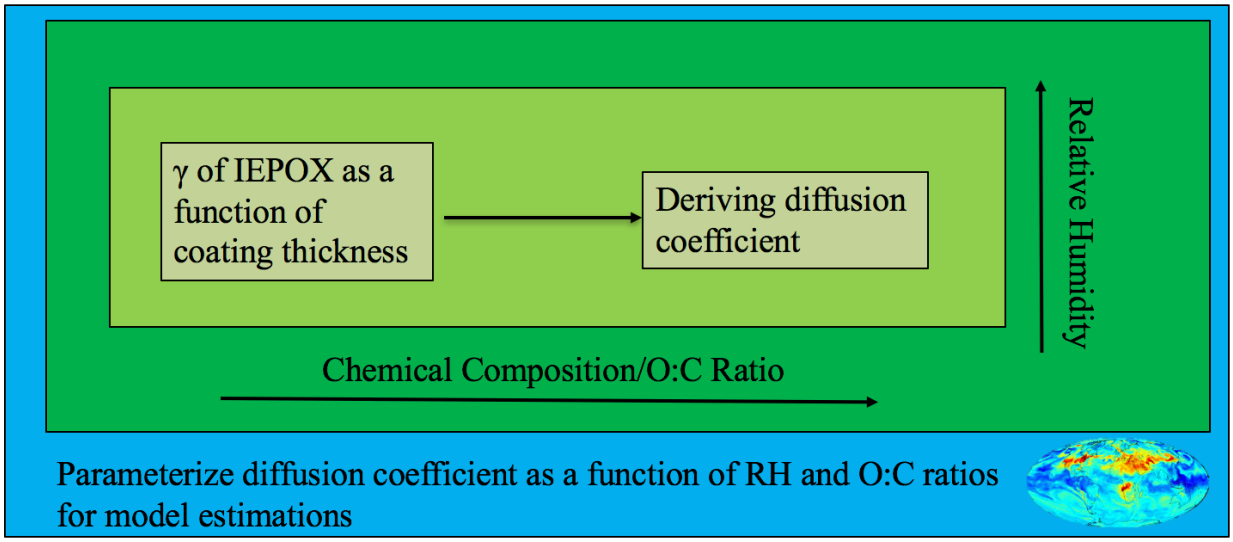

Figure 14 Schematic chart on future plans for the project. Firstly, the uptake coefficients with different coating thickness are utilized to derive the diffusion coefficient of a specific condition. Then the diffusion coefficients are calculated as a function of the chemical composition and the relative humidity. Lastly, the diffusion coefficients are parameterized for a more general modeling estimations on how organic coating affects the overall SOA multiphase production.

Task 3 Implementation in an air quality model

Introduction

The chemical pathway for isoprene-derived SOA begins with reactions with the hydroxyl radical (OH) under low-nitric oxide (NO) conditions producing isoprene hydroxyl hydroperoxide (ISOPOOH). ISOPOOH can then further react with OH to form isoprene epoxydiols (IEPOX) that partition onto pre-existing aerosol seed forming IEPOX-derived SOA [5-13]. Most of the SOA products have been identified as: C_5-alkene triols [42], 2-methyl tetrols [6], IEPOX-organosulfate [43, 44], cis-/trans-3-MeTHF-3,4 diols [8, 45], IEPOX dimers [46], organosulfate of dimer, brown carbon[47], $ISOP(OOH)_2$, organosulfate, 2-methylglyceric acid, and dimeric esters [48]. Based on this work it is now known that IEPOX-SOA formation is affected by several physical and chemical parameters that include: aerosol acidity, relative humidity (RH), diffusion in particle phase, particle reactivity, and the capability that existing aerosol seeds can absorb mass [15]. Thus, high RH conditions in the presence of acidified inorganic aerosols are ideal for this production of aerosols in the atmosphere [6]. Once IEPOX-SOA is formed it also undergoes further reactions increasing $PM_{2.5}$ mass.

The IEPOX-derived SOA have recently been added to the 5.1 version of the Community Multiscale Air Quality Model (CMAQ) via a heterogeneous reaction parametrization. Using this parameterization of the CMAQ model can now explicitly predict two known SOA tracers: 2-methyltetrols (tetrols) and organosulfates (IEPOXOS). This parameter-based method provided a modeling framework used in this work to predict isoprene SOA. Although a framework exists, many of the parameters remain uncertain and it also does not include the impacts of existing SOA coatings in acidic sulfate aerosol. Thus, the focus of this work is to implement a model to also include the impact that organic SOA coatings could have on uptake parameters of IEPOX. In the real atmosphere, aerosol seed can be coated by organic layers formed by oxidation of VOCs that will change the physical and chemical properties of the existing aerosol. Therefore, a more accurate IEPOX-SOA prediction should be achieved by including the effects of existing SOA coatings into the heterogeneous reactive uptake method. The goal of this task was to implement an updated coatings algorithm and evaluate the predicted changes in IEPOX-SOA.

Given the complexity of the analysis this task focused on implementing the heterogeneous reaction parametrization algorithms in a 0-D model. Using the 0-D model allowed for an efficient tool to investigate parameter uncertainty. All modeling runs were evaluating against field measurements taken during the 2013 SOAS campaign at the Look Rock (LRK), Tennessee ground site. At this site the Aerodyne high-resolution time-of-flight chemical ionization mass spectrometry (HR-ToF-CIMS) was used to provide the estimation of gas phase IEPOX concentration [49]. The Aerodyne Aerosol Chemical Speciation Monitor (ACSM) measured the inorganic

sulfate, nitrate, ammonium, and chloride aerosol mass concentrations. Other environmental variables that were measured included ambient temperature and RH. These variables were used to predict aerosol liquid water content and pH using the ISORROPIA thermodynamic model [50]. Aerosol surface area and particle size distributions were provided by aerosol sizing instrumentation at the site [49]. As shown here, these evaluations with the 0-D model has for the first time quantified the potential impacts of coatings on IEPOX-SOA formation.

Methods

Field Measurements

Field measurements at LRK ground site during SOAS provided inputs for the model simulations and the IEPOX SOA tracer concentrations needed for model evaluation. Ambient temperature, RH and aerosol concentrations were obtained from measurements [12]. The sum of IEPOX and its gas-phase precursor ISOPOOH were detected as $[CH_3COO{\cdot}C_5H_{10}O_3]^-$ ion at m/z 177 by Aerodyne high-resolution time-of-flight chemical ionization mass spectrometry (HR-ToF-CIMS) using acetate reagent ion chemistry [51]. Tetrols and IEPOXOS were also quantified during the 2013 SOAS campaign at the LRK ground site [12]. The $PM_{2.5}$ samples were collected onto prebaked Tissuquartz filters (Pall Life Sciences, 8x10 in) with three high-volume $PM_{2.5}$ samplers (Tisch Environmental, Inc.). Each sampler collected $PM_{2.5}$ every 3 hours during the high-NOx and SOx periods (intensive sampling periods), and every 11 hours during the low-NOx and SOx periods (regular sampling periods). From each filter two 37 mm punches were extracted in separate pre-cleaned scintillation vials with 20 mL high-purity methanol (LC-MS Chromasolv-grade, Sigma-Aldrich) by sonication for 45 minutes. One punch was used for analysis by gas chromatography interfaced to an electron impact-mass spectrometer (GC/EI-MS) and the other one was used for ultra-performance liquid chromatography coupled to both diode array detection and high-resolution quadrupole time-of-flight electrospray ionization mass spectrometry (UPLC/DAD-ESI-HR-QTOFMS).

Tetrol concentrations were analyzed by GC/EI-MS (Hewlett-Packard (HP) 5890 Series II Gas Chromatograph equipped coupled to an HP 5971A Mass Selective Detector) with prior trimethylsilylation of filter extracts by reaction with 100 µL of BSTFA + TMCS (99:1, v/v, Supelco) and 50 µL of pyridine (anhydrous, 99.8%, Sigma-Aldrich) at 70 °C for 1 h. Tetrols were quantified using authentic standards synthesized in-house [12]. IEPOXOS concentrations were analyzed by UPLC/DAD-ESI-HR-QTOFMS (Agilent 6500 series system equipped with a Waters Acquity UPLC HSS T3 column) with prior reconstitution of filter residues in 150 µL of a 50:50 (v/v) solvent mixture of methanol (LC-MS Chromasolv-grade, Sigma-Aldrich) and laboratory Milli-Q water (18.2 MΩ). IEPOXOS were quantified using an authentic standard synthesized in-house [12].

0-D Model and Reactive uptake

Based on the finding in Task 2 that suggested that α-pinene SOA coated acidic sulfate particles has a core-shell morphology the modeling approach adopted for this work was a resistor organic coating model from Gaston et al. [2014]. In summary, the model assumes that the formation of IEPOX-SOA is predicted as a first order heterogeneous reaction:

$$IEPOX_{(g)} \rightarrow IEPOXSOA_{(aerosol)} \quad (3)$$

In this first order heterogeneous reaction, the rate constant k_{het} is defined as

$$k_{het} = \frac{SA}{\frac{r_p}{D_g}+\frac{4}{\nu y}} \quad (4)$$

where SA is the aerosol surface area ($\mu m^2/cm^3$), ν is the mean molecular speed (m/s) in the gas phase, r_p is the effective molecular particle radius (cm), D_g is IEPOX diffusivity in the gas phase, and MW is the molecular weight of IEPOX (118 g/mol). The y is the parameterized heterogeneous reactive uptake as defined in equation 5 [14].

$$\frac{1}{\gamma} = \frac{1}{\alpha} + \frac{\nu}{4H*R*T\sqrt{D_a*k_{particle}}}\frac{1}{\coth(q)-\frac{1}{q}} + \frac{\nu*l_{coat}*r_{part}}{4*H_{coat}*R*T*D_{org}*r_{core}} \quad (5)$$

where α is the accommodation coefficient, H is the Henry's Law coefficient (M/atm), R is the gas constant, T is temperature (K), D_a is the diffusivity in the aerosol phase, and q is the diffuso-reactive parameter defined in equation 6.

$$q = (r_p\sqrt{\frac{k_{particle}}{D_a}}) \quad (6)$$

In Equation 5 $k_{particle}$ is also treated as a pseudo-first order rate constant (s^{-1}) and is calculated by assuming protonation of the IEPOX and nucleophilic addition as defined in equation 7.

$$k_{particle} = k_{H^+,water}a_{H^+}LWC + k_{HSO_4^-,water}[HSO4^-]LWC + k_{NH_4^+,water}[NH_4^+]LWC + k_{H^+,SO_4^{2-}}a_{H^+}[SO_4^{2-}] \quad (7)$$

The third term in equation 5 accounts for the influence of coatings. In this third term H_{coat} is the effective Henry's Law constant for an organic coating and l_{coat} is the organic coating thickness (m). l_{coat} has not been measured thus an initial estimation of coating thickness was made of 10% of total aerosol seed radius as shown in equation 8.

$$l_{coat} = 0.1 * r_p \quad (8)$$

In equation 5 r_{core} is the aerosol seed radius (m) and is defined in equation 9.

$$r_{core} = r_p - l_{coat} \quad (9)$$

D_{org} is the coating diffusivity ($m^2\ s^{-1}$) and is defined in equation 10 [52, 53]. The experimental data used in equation 8 was conducted under a RH range of 15% to 70% and an extrapolation of the diffusion coefficient was used when RH was less than 15%. When RH is greater than 70%, coating diffusion will act like water and it was assumed that the diffusion coefficient equals D_a.

$$D_{org} = \mathrm{e}^{-6.55*RH-34.49} \quad when\ RH < 70\% \quad (10)$$

$$D_{org} = 1.0e^{-9}\ m^2 s^{-1}\ (value\ of\ D_a) \quad when\ RH > 70\%$$

Equation 11 is used to define speciation between the 2 different SOA products, IEPOX organosulfate (IEPOXOS), and tetrols based on the relative rates of precursor conversion.

$$IEPOXSOA = \beta * IEPOXOS + (1 - \beta) * tetrols \quad (11)$$

This conversion rate β is defined by fraction of sulfate conversion against total $k_{particle}$ as shown in equation 12.

$$\beta = \frac{k_{H^+,SO_4^{2-}} a_{H^+} [SO_4^{2-}]}{k_{particle}} \quad (12)$$

0-D Simulation Parameters

The equations described above were implemented in a 0-D model via Matlab software version 2017a and the model was used to predict hourly average concentrations for tetrols and IEPOXOS. Based on previous work, a 6-hour model run was used to estimate the final concentration output of the tracers [51]. For example, to estimate the IEPOXOS concentrations for 6 pm a modeling run was initialized at noon and only the final hour of that 6-hour run was used in the analysis.

Simulations were completed for 06/01/2013 to 07/15/2013 relying on SOAS 2013 field measurement at the Look Rock, Tennessee site for input into the 0-D model. Using this input data, a total of two simulations were completed that included a “Base” run where IEPOX SOA formation was predicted by equation 5, but without the third term. In the

second simulation, labelled Base_coat, the full equation 5 with coating impacts was used. For both simulations, the gas phase IEPOX concentration was provided every 30 minutes and the SA and r_p terms were also taken from the measurement data. A D_g value of 8.5e-4 (m^2/s) was the same for both simulations [15] and ν estimated by the root mean square of the measured speed [54]. An α of 0.2 [55] and H of 3.0e7 ($M\ atm^{-1}$) [14, 15, 51, 56] was also assumed for both modeling simulations. T was taken from measurement data and the D_a was estimated as $1.0e^{-9}$ ($m^2\ s^{-1}$) [14, 15, 51, 56]. Predictions by the ISORROPIA [57] program with measurements were used for both simulations to calculate the parameters needed for the $K_{particle}$ as defined in equation 7. For the Base_coat simulation the l_{coat} was calculated based on equation 8, r_{core} used equation 9, and D_{org} relied on equation 10 where RH was taken from the measurement data. Finally, an H_{coat} value of 3.0e-1 ($M\ atm^{-1}$) was used in the Base_coat simulation [14].

Results

The output of the 0-D simulations were evaluated against 3 and 11 hour averaged filters collected during SOAS at the LRK ground site. For each filter the predicted SOA was also averaged to match the filter start and end times. Figure 15 shows the predicted tetrol concentrations from the Base and Base_coat simulations paired with the measurement data for 6/1 to 7/15. In the measured tetrol data there is an observed diurnal pattern and the highest peaks of 1.6 ug/m^3 occur early in the field campaign. Both simulations can predict this diurnal pattern and match the timing of the tetrol peaks. The Base simulation does tend to overpredict the larger peaks by as much as 73% on June 13th. In the latter half of the field campaign measured tetrols rarely reached 0.4 ug/m^3 and the Base model tended to underpredict these values by as much as 99%. Due to both the under and over predictions the NMB for this evaluation was -4.5% as shown in Table 7, but the NME of 83.4% more accurately reflects the inability to match the observed data.

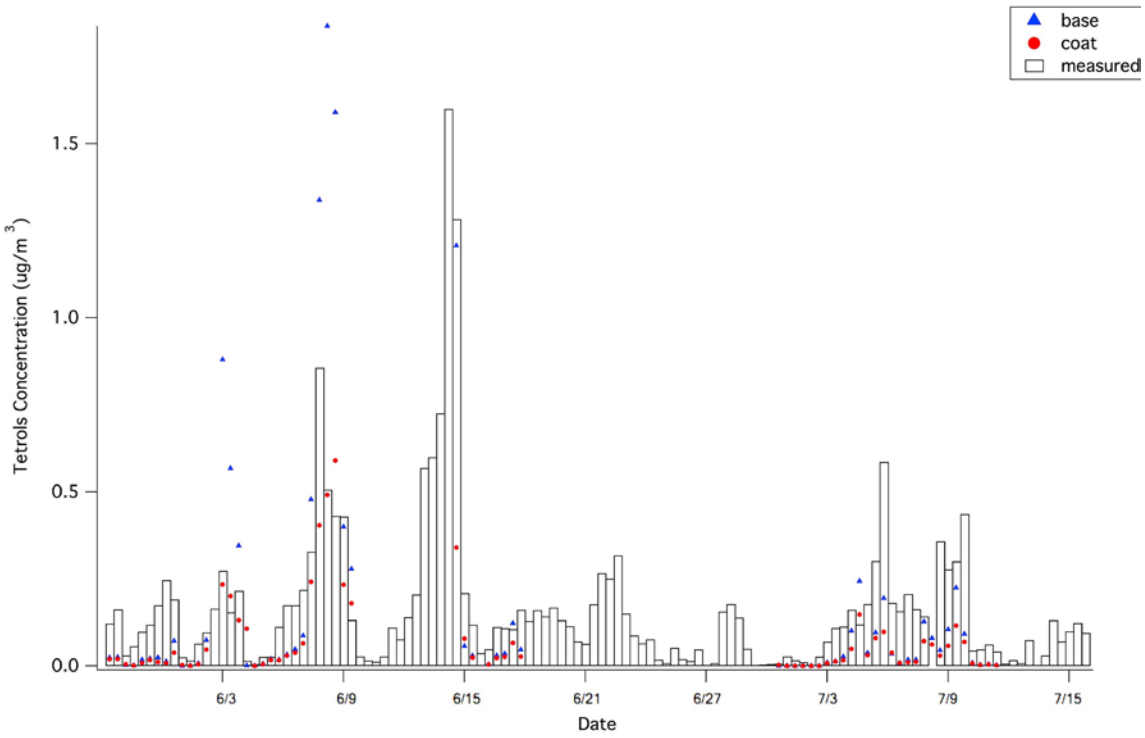

Figure 15 Tetrols concentrations (ug/m^3) measured (boxes) at Look Rock ground site and predicted in the Base (blue) and Base_coat (red) simulations.

Table 7 Model performance of NMB and NME against observations from the Look Rock ground site.

	Tetrol		IEPOXOS	
	Base	Base_coat	Base	Base_coat
NMB (%)	-4.5	-60.2	-73.6	-89.4
NME (%)	83.4	67.6	75.7	89.4

Figure 15 also shows the impact that the addition of the organic coating term has on predicted tetrol concentrations. In comparison with all Base predictions the Base_coat predicted an average 29% reduction in tetrol concentrations. This reduction resulted in poorer performance when the Base model underpredicted tetrols, but also many of the overprediction in the Base model were now underpredictions. As a result of these reductions Table 7 shows NMB worsening to -60.2%. The Base_coat model did reduce the NME when compared with the Base model by 21% showing an improvement in error with the inclusion of an existing organic coating.

As shown in Figure 16, the IEPOXOS concentrations were observed to have a similar temporal pattern as the measured tetrols. The impact of organic coatings here is also significant with an average 31% reduction. This reduction in predicted IEPOXOS concentration increased NMB by 16% and increased NME by 14%. The amount of SOA

generated by is directly impacted by changes in the reactive uptake parameter of IEPOX. Figure 17 shows the percent change in model predicted reactive uptake parameter of IEPOX for both the Base and Base_coat simulations binned by the measured RH. It is clear that when RH equals 70% that the coatings effect is negligible. This is mainly due to the D_{org} relationship in the model that equates D_{org} with D_a when RH is greater than 70%.

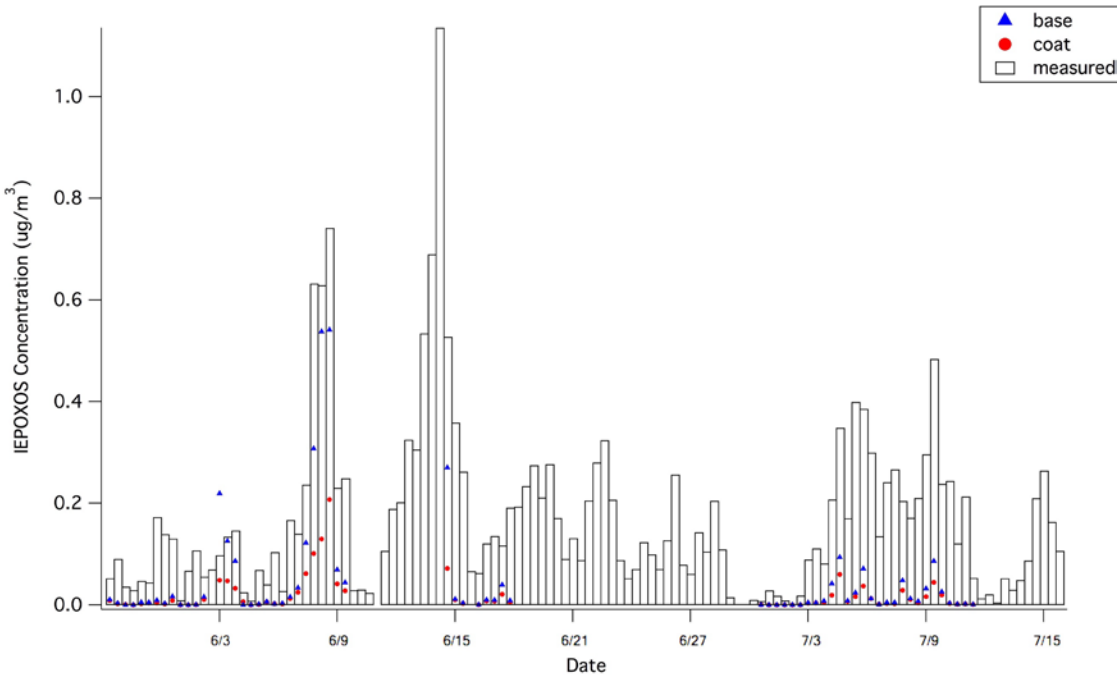

Figure 16 IEPOXOS concentrations (ug/m^3) measured (boxes) at Look Rock ground site and predicted in the Base (blue), and Base_coat (red) simulations.

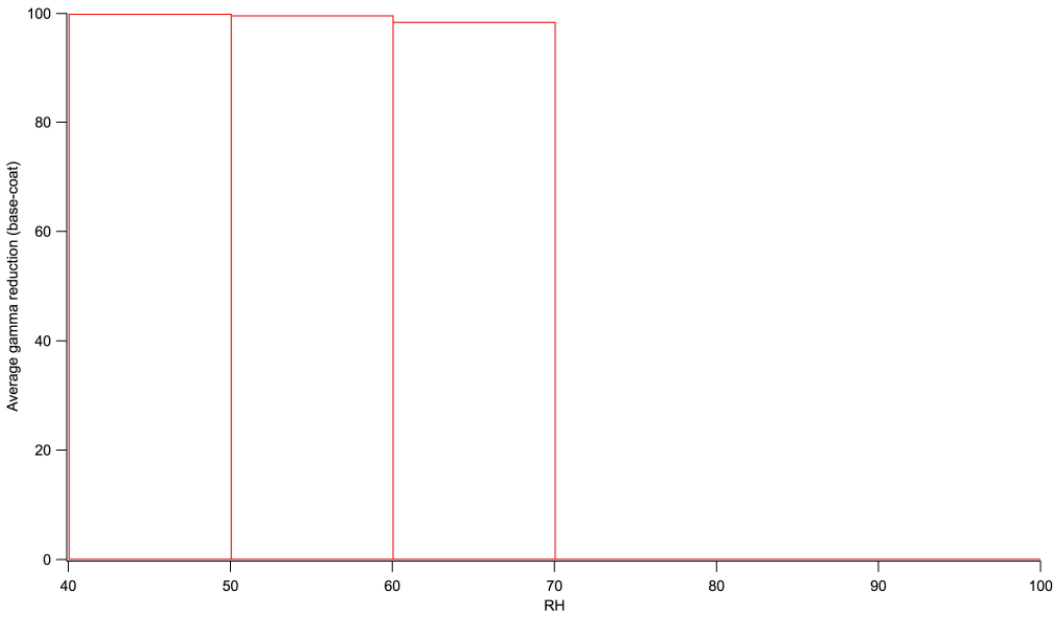

Figure 17 The percent change in model predicted reactive uptake parameter of IEPOX for both the Base and Base_coat simulations binned by the measured RH.

Audits of Data Quality

To ensure data quality the team ran solvent blanks, blank experiments, and calibrations each time experiments were conducted. Also, filters were spiked with authentic standards to determine exact extraction efficiencies from collected filters. Filters were used to quantify the isoprene SOA constituents used for the modeling work. Instruments were always calibrated before each experimental run with the appropriate authentic standards for the target analytes. Blank experiments were conducted to ensure that no compounds were present in the chamber. No isoprene SOA constituents or IEPOX were found in the blank experimental runs. Similar experiments were also conducted for the flow reactor and no SOA or IEPOX was observed in these as well.

For model runs, the quality of the data was ensured by comparing directly to the quantified isoprene SOA tracers and gas phase concentrations. The installation of the software was verified by comparing generated output with concentrations predicted by a separate modeling tool and with the peer reviewed literature. One graduate student, Dr. Surratt, and Dr. Vizuete independently spot-checked the implemented code. Only the graduate student ran simulations while other researchers quality assured the code. All model building was completed in increments starting with simplified cases. At each stage of this development a minimum of 10% of the produced data would undergo a spot check. In this case, a spot check is defined as an independent verification of the generated output by another software system. This was accomplished either by excel spreadsheet for simpler calculations to comparisons with existing runs using different modeling systems. Independent researchers not involved with the collection audited 10% of all measurement data and all calculations were redone in separate software.

Conclusion

The work produced here focused on improving air quality model's ability to predict biogenic derived organic aerosols. Specifically, the multiphase chemical pathway that occurs under low-NOx conditions that produce isoprene derived secondary organic aerosols. The production of these aerosols has implications in Texas given the large isoprene sources and abundance of anthropogenic sources found there. The project hypothesis was that the physical and chemical state of existing aerosol has a range of atmospherically-important effects on IEPOX SOA formation. The hypothesis was tested via laboratory results to derive kinetics information, and constrained 0-D models to reduce parameter uncertainties.

The experimental and modeling results show that particle state would limit multiphase chemistry and subsequently affect the growth and evolution of IEPOX-derived SOA. The experimental data provided new understanding of how SOA coating alters the heterogeneous reactive uptake of IEPOX onto acidic sulfate particles and the influence of humidity, chemical composition, and coating thickness. These modeling results also show that a resistant organic layer produces a reduction in the heterogeneous reactive uptake coefficient, consistent with laboratory findings.

Future Work

Future efforts are now focused on an improved understanding on how the thickness of the existing organic layer mixed with acidic sulfate aerosol and RH influence the reactive uptake coefficient of IEPOX. By correlating the diffusion coefficient with the chemical species information derived from the ACSM, LC/ESI-HR-QTOFMS, and GC/EI-MS, the model developed here could use a parameterized diffusion coefficient correlated with aerosol chemical information (such as O:C and H:C ratios). This could then be applied into a regional scale model to estimate the effects of existing organic coatings on aerosol multiphase chemistry of IEPOX and the resultant $PM_{2.5}$ mass loading. Immediate efforts are being made to further investigate how changes in the SAPRC16 mechanism is affecting radical and NOx budgets.

References

1. Guenther, A., et al., *Estimates of global terrestrial isoprene emissions using MEGAN (Model of Emissions of Gases and Aerosols from Nature).* Atmospheric Chemistry and Physics, 2006. **6**: p. 3181-3210.
2. Carter, W.P.L. *Preliminary SAPRC-16 Atmospheric Chemical Mechanism*. 2017; Available from: http://www.cert.ucr.edu/~carter/SAPRC/16/.
3. Carter, W.P.L., *Development of SAPRC-07 Chemical Mechanism and Updated Ozone Reactivity Scales, Final Report to California Air Resources Board Contract No. 03-318*. 2010.
4. Carter, W.P.L., *DEVELOPMENT OF A CONDENSED SAPRC-07 CHEMICAL MECHANISM Report to the California Air Resources Board Contract No. 05-750*. 2010, University of California Riverside.
5. Paulot, F., et al., *Unexpected Epoxide Formation in the Gas-Phase Photooxidation of Isoprene.* Science, 2009. **325**(5941): p. 730-733.
6. Surratt, J.D., et al., *Reactive intermediates revealed in secondary organic aerosol formation from isoprene.* Proceedings of the National Academy of Sciences of the United States of America, 2010. **107**(15): p. 6640-6645.
7. Zhang, H., et al., *Effect of relative humidity on SOA formation from isoprene/NO Photooxidation: role of particle-phase esterification under dry conditions.* Atmospheric Chemistry and Physics Discussions, 2011. **11**: p. 5407-5433.
8. Lin, Y.-H., et al., *Isoprene Epoxydiols as Precursors to Secondary Organic Aerosol Formation: Acid-Catalyzed Reactive Uptake Studies with Authentic Compounds.* Environmental Science & Technology, 2012. **46**(1): p. 250-258.
9. Lin, Y.H., et al., *Investigating the influences of SO2 and NH3 levels on isoprene-derived secondary organic aerosol formation using conditional sampling approaches.* Atmospheric Chemistry and Physics, 2013. **13**(16): p. 8457-8470.
10. Nguyen, T.B., et al., *Organic aerosol formation from the reactive uptake of isoprene epoxydiols (IEPOX) onto non-acidified inorganic seeds.* Atmospheric Chemistry and Physics, 2014. **14**(7): p. 3497-3510.
11. Krechmer, J.E., et al., *Formation of Low Volatility Organic Compounds and Secondary Organic Aerosol from Isoprene Hydroxyhydroperoxide Low-NO Oxidation.* Environmental Science & Technology, 2015. **49**(17): p. 10330-10339.
12. Budisulistiorini, S.H., et al., *Examining the effects of anthropogenic emissions on isoprene-derived secondary organic aerosol formation during the 2013 Southern Oxidant and Aerosol Study (SOAS) at the Look Rock, Tennessee ground site.* Atmospheric Chemistry and Physics, 2015. **15**(15): p. 8871-8888.
13. Rattanavaraha, W., et al., *Assessing the Impact of Anthropogenic Pollution on Isoprene-Derived Secondary Organic Aerosol Formation in PM2.5 Collected from the Birmingham, Alabama Ground Site During the 2013 Southern Oxidant and Aerosol Study.* Atmospheric Chemistry and Physics, 2016. **15**(15): p. 8871-8888.
14. Gaston, C.J., et al., *Reactive Uptake of an Isoprene-Derived Epoxydiol to Submicron Aerosol Particles.* Environmental Science & Technology, 2014. **48**(19): p. 11178-11186.

15. Pye, H.O., et al., *Epoxide pathways improve model predictions of isoprene markers and reveal key role of acidity in aerosol formation.* Environ Sci Technol, 2013. **47**(19): p. 11056-64.
16. Hutzell, W.T., et al., *Interpreting predictions from the SAPRC07 mechanism based on regional and continental simulations.* Atmospheric Environment, 2012. **46**: p. 417-429.
17. Xie, Y., et al., *Understanding the impact of recent advances in isoprene photooxidation on simulations of regional air quality.* Atmospheric Chemistry and Physics, 2013. **13**(16): p. 8439-8455.
18. Chen, Y.Z., et al., *Assessment of SAPRC07 with updated isoprene chemistry against outdoor chamber experiments.* Atmospheric Environment, 2015. **105**: p. 109-120.
19. Carter, W.P.L., *Development of the SAPRC-07 chemical mechanism.* Atmospheric Environment, 2010. **44**(40): p. 5324-5335.
20. Carter, W.P.L., *Development of a condensed SAPRC-07 chemical mechanism.* Atmospheric Environment, 2010. **44**(40): p. 5336-5345.
21. Jeffries, H.E., D.L. Fox, and R.M. Kamens, *Outdoor Smog Chamber Studies: Light Effects Relative to Indoor Chambers.* Environmental Science and Technology, 1976. **10**(10): p. 1006-1011.
22. Jeffries, H., I. Voicu, and K. Sexton, *Experimental Tests of Reactivity and Re-evaluation of the Carbon Bond Four Photochemical Reaction Mechanism*. 2002, US EPA.
23. Parikh, H.M., et al., *Evaluation of aromatic oxidation reactions in seven chemical mechanisms with an outdoor chamber.* Environmental Chemistry, 2013. **10**(3): p. 245-259.
24. Jeffries, H.E., *Photochemical Air Pollution: Chapter 9*, in *Composition, Chemistry, and Climate of the Atmosphere*, H.B. Singh, Editor. 1995, Van Nostand-Reinhold: New York. p. 308-348.
25. Jimenez, J.L., et al., *Evolution of Organic Aerosols in the Atmosphere.* Science, 2009. **326**(5959): p. 1525-1529.
26. Schobesberger, S., et al., *Molecular understanding of atmospheric particle formation from sulfuric acid and large oxidized organic molecules.* Proc Natl Acad Sci U S A, 2013. **110**(43): p. 17223-8.
27. Kroll, J.H., et al., *Carbon oxidation state as a metric for describing the chemistry of atmospheric organic aerosol.* Nature Chemistry, 2011. **3**(2): p. 133-139.
28. Kroll, J.H., et al., *Secondary organic aerosol formation from isoprene photooxidation.* Environmental Science & Technology, 2006. **40**(6): p. 1869-1877.
29. Liu, J.M., et al., *Brown carbon in the continental troposphere.* Geophysical Research Letters, 2014. **41**(6): p. 2191-2195.
30. Saukko, E., et al., *Humidity-dependent phase state of SOA particles from biogenic and anthropogenic precursors.* Atmospheric Chemistry and Physics, 2012. **12**(16): p. 7517-7529.
31. Virtanen, A., et al., *An amorphous solid state of biogenic secondary organic aerosol particles.* Nature, 2010. **467**(7317): p. 824-7.
32. Vaden, T.D., et al., *Evaporation kinetics and phase of laboratory and ambient secondary organic aerosol.* Proceedings of the National Academy of Sciences of the United States of America, 2011. **108**(6): p. 2190-2195.

33. Cappa, C.D. and K. Wilson, *Evolution of organic aerosol mass spectra upon heating: implications for OA phase and partitioning behavior.* Atmos. Chem. Phys., 2011. **11**(5): p. 1895-1911.
34. Wilson, T.W., et al., *Glassy aerosols with a range of compositions nucleate ice heterogeneously at cirrus temperatures.* Atmos. Chem. Phys., 2012. **12**(18): p. 8611-8632.
35. Baustian, K.J., et al., *State transformations and ice nucleation in amorphous (semi-)solid organic aerosol.* Atmos. Chem. Phys., 2013. **13**(11): p. 5615-5628.
36. Schill, G.P. and M.A. Tolbert, *Heterogeneous ice nucleation on phase-separated organic-sulfate particles: effect of liquid vs. glassy coatings.* Atmos. Chem. Phys., 2013. **13**(9): p. 4681-4695.
37. Wang, B., et al., *Reactivity of liquid and semisolid secondary organic carbon with chloride and nitrate in atmospheric aerosols.* J Phys Chem A, 2015. **119**(19): p. 4498-508.
38. Palm, B.B., et al., *Secondary organic aerosol formation from in situ OH, O3, and NO3 oxidation of ambient forest air in an oxidation flow reactor.* Atmos. Chem. Phys., 2017. **17**(8): p. 5331-5354.
39. Hallquist, M., et al., *The formation, properties and impact of secondary organic aerosol: current and emerging issues.* Atmospheric Chemistry and Physics, 2009. **9**(14): p. 5155-5236.
40. Koop, T., et al., *Glass transition and phase state of organic compounds: dependency on molecular properties and implications for secondary organic aerosols in the atmosphere.* Phys Chem Chem Phys, 2011. **13**(43): p. 19238-55.
41. Weber, R., et al., *High aerosol acidity despite declining atmospheric sulfate concentrations over the past 15 years.* Nature Geoscience, 2016. **9**(4): p. 282-285.
42. Wang, W., et al., *Characterization of oxygenated derivatives of isoprene related to 2-methyltetrols in Amazonian aerosols using trimethylsilylation and gas chromatography/ion trap mass spectrometry.* Rapid Communications in Mass Spectrometry, 2005. **19**(10): p. 1343-1351.
43. Froyd, K.D., et al., *Contribution of isoprene-derived organosulfates to free tropospheric aerosol mass.* Proceedings of the National Academy of Sciences of the United States of America, 2010. **107**(50): p. 21360-21365.
44. Liao, J., et al., *Airborne measurements of organosulfates over the continental U.S.* J Geophys Res Atmos, 2015. **120**(7): p. 2990-3005.
45. DeCarlo, P.F., et al., *Field-deployable, high-resolution, time-of-flight aerosol mass spectrometer.* Anal Chem, 2006. **78**(24): p. 8281-9.
46. Surratt, J.D., et al., *Chemical composition of secondary organic aerosol formed from the photooxidation of isoprene.* J Phys Chem A, 2006. **110**(31): p. 9665-90.
47. Lin, Y.H., et al., *Light-absorbing oligomer formation in secondary organic aerosol from reactive uptake of isoprene epoxydiols.* Environ Sci Technol, 2014. **48**(20): p. 12012-21.
48. Lin, Y.H., et al., *Epoxide as a precursor to secondary organic aerosol formation from isoprene photooxidation in the presence of nitrogen oxides.* Proceedings of the National Academy of Sciences of the United States of America, 2013. **110**(17): p. 6718-6723.
49. Budisulistiorini, H., et al., *Seasonal characterization of submicron aerosol chemical composition and organic aerosol sources in the southeastern United States: Atlanta,*

Georgia and Look Rock, Tennessee. Atmospheric Chemistry and Physics Discussions, 2015. **15**(16).
50. Nenes, A., S.N. Pandis, and C. Pilinis, *Continued development and testing of a new thermodynamic aerosol module for urban and regional air quality models.* Atmospheric Environment, 1999. **33**(10): p. 1553-1560.
51. Budisulistiorini, H., et al., *Simulating Aqueous-Phase Isoprene-Epoxydiol (IEPOX) Secondary Organic Aerosol Production During the 2013 Southern Oxidant and Aerosol Study (SOAS).* Envionmental Science & Technoloy, 2017. **51**(9).
52. Zhang, H., et al., *Secondary Organic Aerosol Formation via 2-Methyl-3-buten-2-ol Photooxidation: Evidence of Acid-Catalyzed Reactive Uptake of Epoxides.* Environ Sci Technol Lett, 2014. **1**(4): p. 242-247.
53. Renbaum-Wolff, L., et al., *Viscosity of alpha-pinene secondary organic material and implications for particle growth and reactivity.* Proc Natl Acad Sci U S A, 2013. **110**(20): p. 8014-9.
54. Raymond, A.S., J.S. Faughn, and C. Vuille, *College Physics, Volume 1*. 9th ed. Vol. 1. 2011.
55. McNeill, V.F., et al., *Aqueous-Phase Secondary Organic Aerosol and Organosulfate Formation in Atmospheric Aerosols: A Modeling Study.* Environmental Science & Technology, 2012. **46**(15): p. 8075-8081.
56. Pye, H.O., et al., *On the implications of aerosol liquid water and phase separation for organic aerosol mass.* Atmos. Chem. Phys., 2017. **17**.
57. Fountoukis, C. and A. Nenes, *ISORROPIA II: a computationally efficient thermodynamic equilibrium model for K+-Ca2+-Mg2+-Nh(4)(+)-Na+-SO42--NO3--Cl--H2O aerosols.* Atmospheric Chemistry and Physics, 2007. **7**(17): p. 4639-4659.